



## Worldwide Linke turbidity information

Jan Remund, Lucien Wald, Mireille Lefèvre, Thierry Ranchin, John Page

► **To cite this version:**

Jan Remund, Lucien Wald, Mireille Lefèvre, Thierry Ranchin, John Page. Worldwide Linke turbidity information. ISES Solar World Congress 2003, Jun 2003, Göteborg, Sweden. International Solar Energy Society (ISES), CD-ROM, 13 p, 2003.

**HAL Id: hal-00465791**

**<https://hal.archives-ouvertes.fr/hal-00465791>**

Submitted on 21 Mar 2010

**HAL** is a multi-disciplinary open access archive for the deposit and dissemination of scientific research documents, whether they are published or not. The documents may come from teaching and research institutions in France or abroad, or from public or private research centers.

L'archive ouverte pluridisciplinaire **HAL**, est destinée au dépôt et à la diffusion de documents scientifiques de niveau recherche, publiés ou non, émanant des établissements d'enseignement et de recherche français ou étrangers, des laboratoires publics ou privés.

## WORLDWIDE LINKE TURBIDITY INFORMATION

### Jan Remund

METEOTEST, Fabrikstrasse 14, CH-3012 Bern, Switzerland,  
+41 (0)31 3072626, +41 (0)31 3072610, e-mail: [remund@meteotest.ch](mailto:remund@meteotest.ch)

### **Lucien Wald, Mireille Lefèvre and Thierry Ranchin**

Ecole des Mines de Paris /Armines, Groupe Teledetection & Modelisation, BP 207, F-06904 Sophia Antipolis cedex ,  
France

### **John Page**

Emeritus Professor of University of Sheffield, Building Science, Sheffield S11 9BG, United Kingdom

**Abstract** – This paper describes the algorithms and data used to construct a worldwide Linke turbidity factor (TL, for an air mass equal to 2) database. Two main steps had to be performed to obtain the information: 1. Assembling estimates of TL and 2. fusing different background layers for the construction of the TL maps. The estimates of TL have two forms: either they stand for specific geographical locations and have a high accuracy, or they are available as gridded data averaged over large areas. Point information was gathered from measured time series of hourly beam and daily global radiation, which were transformed to TL. From publications and networks like AERONET other turbidity quantities were obtained and transformed to TL. The basic gridded data are the maps of daily global irradiation supplied by the NASA-Langley Research Center. The included monthly clear sky irradiances were converted to TL with the same method as for the ground sites. Further gridded information was taken from NOAA pathfinder aerosol data and NASA NVAP. An algorithm was devised to fuse these two types of data and to produce gridded maps in a canonical projection and 5' arc angle cells. These final maps should reproduce the values observed at specific locations. The root mean square error of the interpolation is 0.73 TL units.

## 1. INTRODUCTION

### 1.1 The Linke turbidity factor

The Linke turbidity factor (TL, for an air mass equal to 2) is a very convenient approximation to model the atmospheric absorption and scattering of the solar radiation under clear skies. It describes the optical thickness of the atmosphere due to both the absorption by the water vapor and the absorption and scattering by the aerosol particles relative to a dry and clean atmosphere. It summarizes the turbidity of the atmosphere, and hence the attenuation of the direct beam solar radiation (WMO, 1981; Kasten, 1996). The larger the TL, the larger the attenuation of the radiation by the clear sky atmosphere.

The direct irradiance on a horizontal surface (or beam horizontal irradiance) for clear sky,  $B_c$ , is given by (Rigollier *et al.* 2000):

$$B_c = I_0 \cdot \varepsilon \cdot \sin \gamma_s \exp(-0.8662 T_L(AM2) \cdot m \cdot \delta_{Rayleigh}(m)) \quad (1)$$

where

- $I_0$  is the solar constant, that is the extraterrestrial irradiance normal to the solar beam at the mean solar distance. It is equal to  $1367 \text{ Wm}^{-2}$ ;
- $\varepsilon$  is the correction used to allow for the variation of sun-earth distance from its mean value;
- $\gamma_s$  is the solar altitude angle.  $\gamma_s$  is  $0^\circ$  at sunrise and sunset;

- $T_L(AM2)$  is the Linke turbidity factor for an air mass equal to 2;
- $m$  is the relative optical air mass;  $m_0$  the optical air mass at sea level.
- $\delta_{Rayleigh}(m)$  is the integrated Rayleigh optical thickness, due to pure molecular scattering.

The pressure correction equation has been newly introduced:

$$\delta_{Rayleigh} = \left[ p_c \cdot \left( \frac{6.625928 + 1.92969 \cdot m_0 - 0.170073 \cdot m_0^2}{0.011517 \cdot m_0^3 - 0.000285 \cdot m_0^4} \right) \right]^{-1}$$

$$m = \frac{p}{p_0} \sqrt{\sin(\gamma_s) + 0.50572 \cdot (57.29578 \cdot \gamma_s + 6.07995)^{-1.6364}}$$

$$m_0 = 1 / \sqrt{\sin(\gamma_s) + 0.50572 \cdot (57.29578 \cdot \gamma_s + 6.07995)^{-1.6364}} \quad (2)$$

$$\frac{p}{p_0} = \exp\left(-\frac{z}{8435.2}\right) \quad (3)$$

$$\begin{aligned}
 p &= p_0 : \\
 p_c &= 1 \\
 \frac{p}{p_0} &= 0.75 : \\
 p_c &= 1.248274 - 0.011997m_0 + 0.000370m_0^2 \\
 \frac{p}{p_0} &= 0.5 : \\
 p_c &= 1.68219 - 0.03059m_0 + 0.000890m_0^2
 \end{aligned} \tag{4}$$

Between the pressure levels the correction factor  $p_c$  is interpolated linearly.

The quantity,  $\exp(-0.8662 T_L(AM2) m \delta_{\text{Rayleigh}}(m))$ , represents the beam transmittance of the beam radiation under cloudless skies. The relative optical air mass  $m$  expresses the ratio of the optical path length of the solar beam through the atmosphere to the optical path through a standard atmosphere at sea level with the sun at the zenith. As the solar altitude decreases, the relative optical path length increases. The relative optical path length also decreases with increasing station height above the sea level,  $z$ .

With the formulation of Grenier (1994) or Rigollier (2000)  $\delta_{\text{Rayleigh}}(m)$  increases with altitude, because of decreasing air mass  $m$ . This error has been eliminated with the new pressure correction  $p_c$ , adapted to SMART2 (Gueymard, 1998) model output. The new formula corresponds to Gueymard's equation at sea level and is very close to the equation of Kasten (1996), used in Rigollier (2000), for sea level altitude.

It is assumed that the integrated optical thickness of the atmosphere is the sum of the integrated optical thicknesses of Rayleigh atmosphere, mixed gases (mainly  $\text{CO}_2$ ,  $\text{O}_2$ ), ozone, aerosol and water vapor:

$$\delta = \delta_{\text{Rayleigh}} + \delta_{\text{gas}} + \delta_{\text{ozone}} + \delta_{\text{aerosol}} + \delta_{\text{water}} \tag{5}$$

With this assumption we can write

$$B_c = I_0 \cdot \varepsilon \cdot \sin \gamma_s \exp(-0.8662 \cdot m \cdot \delta(m)) \tag{6}$$

The attenuation caused by the aerosols and the water vapor is known as the turbidity of the atmosphere. The Linke turbidity factor  $T_L$  is:  $T_L = \frac{\delta}{\delta_{\text{Rayleigh}}}$  (7)

In the past, different types of TL values were used. Grenier (1994) introduced a new formula of Rayleigh optical thickness, which corrected the influence of air mass and led to a lowering of TL of an average of 15 %. We decided to use the original Kasten TL for air mass 2, which is simply:

$$T_L(AM2) = \frac{1}{0.8662} T_L(\text{Grenier}) \tag{8}$$

For altitude correction of TL the pressure equation is used:

$$T_L(z) = T_L(0) \frac{p}{p_0} \tag{9}$$

## 1.2 Methodology

Several data sets of the Linke turbidity factor are available. They are either values for specific geographical sites or are available as gridded data. The values for specific sites are accurate but have a limited extension in space. The gridded values cover the whole world.

The principle is to fuse these two different sets of information in order to obtain the final product on a grid with cells of 5' in size. D'Agostino, Zelenka (1992), Zelenka et al. (1992) and Zelenka, Lazic (1987) proposed solutions to such a problem. In a case similar to ours, since they used the same gridded data, Beyer *et al.* (1997) proceed as follows: The original gridded data set is resampled by the means of a bicubic spline and re-gridded with a regular cell size of 5' x 5' in a canonical projection. It is then assumed that the value in a cell should be equal to the mean of those observed for the measuring stations within the cell.

For all cells containing at least a measuring station, the difference between both data sets is computed. Then, these differences are interpolated by the means of a linear unbiased interpolator. The authors above-mentioned have employed Kriging or co-Kriging. The distance for interpolation takes into account the orography. Once the field of the residuals is obtained for each cell, this field is added to the gridded data, providing an unbiased gridded map.

The methodology that we used in the construction of our maps of the Linke turbidity factor is derived from that of Beyer *et al.* (1997). The main drawbacks of the previous method lies in the fact that the gridded data that are fused with the sites observations at cells of 5' in size result from an interpolation of the gridded data at cells of 280 km in size. Accordingly, there are no high frequencies in the gridded data at 5', and more exactly, there are no wavenumbers comprised between 5' and 150' of arc angle.

Therefore, the gridded data is very smooth with the exception of some high frequencies which are locally injected by fusing with sites observations. The method was appropriate in the case of Beyer *et al.* because a large number of sites observations were available. It is not appropriate in our case however, because large areas are without site observations.

## 2. DATA

The estimates of the Linke turbidity factor, TL, have two forms: either they stand for specific geographical locations or they are available as gridded data averaged over large areas. The values for specific sites are accurate but have a limited extension in space. The gridded values cover the whole world. They are available for cells of 280 x 280 km<sup>2</sup> and are space-averaged.

Remund J., Wald L., Lefevre M., Ranchin T., Page J., 2003. Worldwide Linke turbidity information. Proceedings of ISES Solar World Congress, 16-19 June, Göteborg, Sweden, CD-ROM published by International Solar Energy Society.

### 2.1 Data for specific locations

We assembled several data sets of the Linke turbidity factor. They originate from publications and available databases or were derived from measurements of other geophysical parameters. For the latter, the major source is made of measurements of daily global irradiation available for several years. By using the ESRA model for the daily irradiation under clear skies (Rigollier *et al.* 2000), a technique providing the Linke turbidity factor was developed. Other data are also investigated, such as visibility, Angström coefficients and hourly beam irradiation (Tab. 1).

Tab. 1: Sources of atmospheric turbidity point information

Name of source	Abbr.	Database
Hourly beam measurements	B	55 sites with hourly beam measurements
Daily global radiation measurements	G	155 sites with daily global radiation measurements
Publications	P/A	80 sites with atmospheric turbidity
Angstrom a and b	AB	ESRA (2000), 595 sites
Visibility (max. per month)	V	Globalsod 1996–2000, 1500 sites

Several authors have shown links between visibility and turbidity (King and Buckius, 1971; Gueymard, 2001). But because of bad quality of visibility measurements and the big local influences (horizon) the data could not been taken into account. TL values calculated with Angstrom a and b values had to be discarded as well due to uncertain quality.

Finally, a total of 268 stations was included. All TL's were calculated first at site altitude. In a second step, the values were reduced to sea level with Eqn. 3 in order to be comparable with the background information.

The list of sites and the results are given in the annex.

### 2.2 Published measurements

7 different sources of published data were found. There are two main groups: One source consists of data of scientific papers (No. 1–6), the other source of published data in the internet (No. 7) (Tab. 2).

Tab. 2: Different sources of published turbidity values

Nr	Source	N	Period
1	Gueymard, C.A. and Garrison J.D. (1998)	5	1977–84
2	Gueymard, C. (1994)	14	1971–86
3	Jacovides, C.P. (1997)	1	1954–92
4	Pedros, R. et al. (1999)	1	1990–96
5	Rapti, A.S. (2000)	1	1973–76
6	B.N.Holben et al. (2000)	23	1993–2000
7	AERONET Download site <a href="http://aeronet.gsfc.nasa.gov/">http://aeronet.gsfc.nasa.gov/</a>	36	1994–2001

### 2.3 The gridded data

The basic gridded data are the maps of daily global irradiation supplied by the NASA-Langley Research Center, in the framework of the Solar Radiation Budget Project SRB (Whitlock 1995; Di Pasquale, Whitlock 1995).

Using a similar technique as for sites observations, the included monthly clear sky irradiances (Staylor approximation) were converted to Linke turbidity with the same method as for the ground sites with daily global radiation time series. This data set only has a low spatial resolution. The cell is an equal area cell everywhere of 280 x 280 km<sup>2</sup>. At mid-latitude, it corresponds to approximately 2.5 x 2.5 degrees<sup>2</sup> of arc angle. The twelve maps (one per month) of TL were re-mapped using the canonical projection. This is performed by the means of the spline bi-cubic operator. A mirror technique is used for the edges. The cells are squared and have a size of 160' of arc angle. This set of worldwide maps is called the set TL<sub>SRB</sub>.

The Thermal Modeling and Analysis Project (TMAP) at NOAA's Pacific Marine Environmental Laboratory was formed in 1985 to advance understanding of the processes that control the evolution of sea surface temperature and upper ocean thermal structure (TMAP, 2001). The server of this project also provides aerosol optical depth at 630 μm for the ocean for several years (1981–00). The aerosol data was transformed to Linke turbidity factor for each cell. Here the equations 16 and 17 were used with water vapour values of NVAP and an assumed α of 1.3.

The twelve maps with means of 1985–99 were re-mapped as described above. The cells are square and have a size of 80' of arc angle. Information is only available over the ocean. Comparisons with available measurements over small islands show that this information from TMAP is reliable.

Within the NVAP (NASA Water Vapor Project), the NASA Langley Research Center Atmospheric Sciences Data Center combined several observations to construct world-wide maps of the content of water vapor integrated over the total column (Randel et al., 1996). The gridded data are available on the internet (NVAP, 2001). We computed the mean value for each cell over the 10 years (1988–97) available for each month (Fig. 1). As seen above, the water vapor has an important impact on TL and these data will be used to modulate the field of TL. They are re-mapped as described above. The cells are square and have a size of 80' of arc angle.

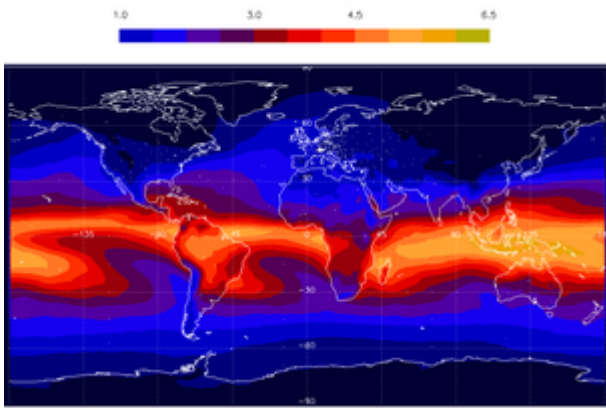


Fig. 1: Total water vapor (TPW) according NVAP in cm. January mean (1988–97).

Maps of aerosol index over land and oceans were constructed by the French space agency (CNES) in the framework of the POLDER-ADEOS mission with grid cells of 10' in size. They are available on the internet (CNES, 2001). Unfortunately, only 8 months of data are available (November 1996–June 1997). This source of information was rejected, because of the shortness of this time-series. This impedes an accurate modelling of the high frequencies of the aerosol distribution. Other sources, such as the MODIS/TERRA project, also have short time period and are not used either.

The last set of data that is used in the synthesis is a digital elevation model with a cell size of 5' of arc angle. This model is the TerrainBase model (1995), constructed by the NOAA National Geophysical Data Center. Over the oceans, the elevation was set to 0 m.

### 3. METHOD

#### 3.1 Method to calculate ground TL values

3.1.1 Method to calculate TL values from beam measurements. The formula (1) was rearranged to determine TL:

$$T_L(\text{AM2}) = \frac{\log\left(\frac{B_c}{I_0 \cdot \varepsilon \cdot \sin \gamma_s}\right)}{(-0.8662 \cdot \delta_{\text{Rayleigh}} \cdot m)} \quad (10)$$

Conditions:

$$B_n \geq 200 \text{ W/m}^2$$

$$k_t = \frac{G_h}{I_0 \cdot \varepsilon \cdot \sin \gamma_s}$$

$$k_t' = k_t / [1.031 \cdot \exp(-1.4/(0.9 + 9.4/m)) + 0.1]$$

$$k_t' \geq 0.7$$

(11)

$$K_t = \frac{\bar{G}_h}{(I_0 \cdot \varepsilon \cdot \sin \gamma_s)}$$

$$K_t \geq 0.4$$

$$\gamma_s \geq 10^\circ$$

All equations for the solar path are taken from ESRA handbook (ESRA, 2000). Several conditions have been used in order not to get beam values influenced by clouds. Without sunshine data it is posteriori very difficult to filter all partially cloudy hours.

According Pedros et al. (1999) only hourly values are used with a sun angle corrected clearness value ( $k_t'$ ) of at least 0.7. Additionally, only hours of days with at least 40% of clear hours and a daily clearness index of at least 0.4 are taken into account.

According Gueymard (1998) it is tested if there are jumps between two adjacent hours. If a value is more than 0.5 units higher than the one the hour before, the value is not taken into account. All hourly values higher than the daily median plus 1 unit are cleared. As monthly value the median of all TL values of a month is taken, because the median value is more robust in respect to outliers. Most often the median value is slightly lower than the mean value.

All values were visually checked. Unreasonable data was flagged and not used.

3.1.2 Method to calculate TL values from daily global radiation measurements. With longer time series of daily mean global radiation and ESRA clear sky model (Rigollier, 2000) it is possible to estimate the Linke turbidity. With an iteration of the ESRA clear sky model (daily integration) TL is estimated. TL is varied until the calculated global radiation value corresponds to the measured value. This is made for the typical day per month for maximum solar radiation.

Two changes were introduced to the model:

1. The new formulation of the Rayleigh optical depth with altitude (Eqns. 2–4) is used.
2. In ESRA (2000) the diffuse formulation did not make an allowance for variations in the site atmospheric pressure as was the case for the beam estimates. Further investigation has shown the desirability of including the pressure correction. Setting  $(T_L^*) = p/p_0 \cdot T_L$

$$D_c = I_0 \cdot \varepsilon \cdot F_d(\gamma_s) \cdot T_{rd}(T_L^*) \quad (12)$$

$$T_{rd}(T_L^*) = -1.5843 \cdot 10^{-2} + 3.0543 \cdot 10^{-2} \cdot T_L^* + 3.797 \cdot 10^{-4} \cdot (T_L^*)^2 \quad (13)$$

$$F_d(y_s) = A_0 + A_1 \cdot \sin \gamma_s + A_2 \cdot \sin^2 \gamma_s \quad (14)$$

$$\begin{aligned} A_0 &= 0.26463 - 0.061581 \cdot T_L^* + 0.0031408 \cdot (T_L^*)^2 \\ A_1 &= 2.04020 + 0.018945 \cdot T_L^* - 0.011161 \cdot (T_L^*)^2 \\ A_2 &= -1.33025 + 0.03231 \cdot T_L^* - 0.0085079 \cdot (T_L^*)^2 \end{aligned} \quad (15)$$

The database with 97% percentile values was compared at Nice and La Rochelle with the 10 years daily values database. The results are very similar to the mean of the highest 6 values out of 10 years. Out of the original 10 sites only 5 sites could be used due to low quality of the data.

Only time series of at least 5 years were considered. First the mean daily maximum clearness index for each month was calculated. For daily values it is even more difficult to filter clouds a posteriori than for hourly values. To avoid taking cloudy days into account, the mean of the 6 highest monthly means out of the 10 years are taken (5 out of 9 years, 4 out of 7 years if less than 10 years are available). Additionally, a lower limit of Kt was set, similar to the hourly values (Eqn. 16). This limits were adapted to the height of sun because the Perez correction of kt is not suitable for very low solar altitudes:

$$\begin{aligned} \text{hsmax} &> 30^\circ \\ K_t &\geq 0.8 \cdot \bar{k}_t \\ 15 < \text{hsmax} &\leq 30^\circ \\ K_t &\geq 0.6 \cdot \bar{k}_t \\ 4 < \text{hsmax} &\leq 15^\circ \\ K_t &\geq 0.4 \cdot \bar{k}_t \end{aligned} \quad (16)$$

With these filters many sites (mainly high latitude sites during winter) could not be calculated because no clear days per month existed. This method is also not suited for tropical and passat zones, where at least during some months no totally clear days exist.

As a minimum value for TL at sea level the following equation was used, which was adapted to the spectral2 model:

$$T_{L\min} = -0.0196 \cdot w^2 + 0.2372 \cdot w + 1.8545 \quad [w \text{ in cm}] \quad (17)$$

If water vapour was measured, w was estimated with dew point temperature.

$$w = \exp(-0.075 + 0.07 \cdot T_d) \quad [w \text{ in cm}] \quad (18)$$

All values were visually checked. Unreasonable data was flagged and not used.

*3.1.3 Method to calculate TL values from published turbidity and aerosol values.* The published data often had to be recalculated in order to get TL values. Mostly Angstrom  $\beta$  values or aerosol optical depth are published. The following formulae are used:

For  $TL_{AM2}$  with  $\beta$  values and precipitable water as input the new equation was made according the spectral2 model:

$$T_L(AM2) = (1.8494 + 0.2425 \cdot w - 0.0203 \cdot w^2) + (15.427 + 0.3153 \cdot w - 0.0254 \cdot w^2) \cdot \beta \quad [w \text{ in cm}] \quad (19)$$

The results are very similar to the output of Dogniaux's (1974) equation for TL, but it is not dependent on airmass and solar altitude. The formula was developed for precipitable water contents between 0.5 and 6 cm,  $\beta$  between 0 and 0.26 and  $\alpha$  equal to 1.3.

With aerosol optical depth and  $\alpha$  as input  $\beta$  can be calculated (Angstrom, 1929):

$$\beta = \frac{\tau_{a\lambda}}{\lambda^{-\alpha}} \quad (20)$$

If more than one wavelength is available  $\alpha$  can be calculated with (Gueymard, 1994):

$$\alpha = \frac{\log(\tau_{a\lambda_2} / \tau_{a\lambda_1})}{\log(\lambda_1 / \lambda_2)} \quad (21)$$

If only one wavelength is available, an  $\alpha$  of 1.3 was assumed.

For AERONET stations, where water vapour is also measured, the wavelengths of 1020  $\mu\text{m}$  and 440  $\mu\text{m}$  were used to determine  $\beta$ . TL Values bigger than 10 were set equal 10. All of the AERONET measurements were made with CIMEL sun/sky radiometers.

### 3.2 Fusion of gridded data

We propose an innovative approach in the fusion of gridded data. The algorithm consists of three steps and takes advantage of two known methods.

In the first step, several gridded data sets which have different spatial resolutions and represent different geophysical parameters are fused in order to construct several approximations of the Linke turbidity factor at increasing spatial resolutions. At the end of the first step, the spatial resolution is 20'.

In the second step, it is assumed that the value in a cell of 20' in size should be equal to the mean of those values observed for the measuring stations within the cell. For all cells containing at least one measuring station, the difference between both data sets is computed. Then, these differences are interpolated by the means of a linear unbiased interpolator. Once the field of the residuals is obtained for each cell, this field is added to the gridded data, providing an unbiased gridded map.

In the last step, the final products are constructed by fusing the gridded data at 20' with orography, using a similar approach as in the first step.

*3.2.1 The wavelet transform and multiresolution analysis.* The algorithm for fusing uses the wavelet transform and the multiresolution analysis. These tools are now briefly described.

The Fourier transform is likely the most known method for spatial analysis. The wavelet transform is a more recent tool, which is a space-wave vector (or time-frequency) transform, while the Fourier transform only provides analysis in the wave vector (or frequency) domain. The wavelet transform may be combined with the multiresolution analysis, and both tools form a convenient means to describe, analyze and model the information contained in an image, or in a series of data.

As the Fourier transform, the wavelet transform performs a decomposition of the signal on a base of elementary functions: the wavelets. For more details about the properties of the wavelets, one can refer to Meyer (1990) or Daubechies (1992).

The multiresolution analysis is a means to describe and model the signal in the time-frequency domain or in the space-wavevector domain or in any domain with similar duality. It makes use of space (or time) transforms or filters. For more information about multiresolution analysis we refer to Remund et al. (2002), Mallat (1989) and Wald and Ranchin (2000).

*3.2.2 The models used.* The original data set is the Linke turbidity factor  $TL_{SRB}$  at a resolution of 160':  $TL_{160}$ . The other data sets are

- the Linke turbidity factor derived from the TMAP data sets,  $TL^{TMAP}_{80}$ , at a resolution of 80',
- the water vapor content at a resolution of 80',  $WV_{80}$ ,
- the orography at a resolution of 5',  $z_5$ .

Two iterations are performed using the new strategy. The resolution is increased from 160' to 80', and then, from 80' to 5'. A final multiresolution analysis provides the data set at 20', the resolution at which the fusion with sites observations is to be performed.

In the first iteration, from 160' to 80', only the data  $WV_{80}$  and  $TL^{TMAP}_{80}$  are used. Though the water vapor data  $WV_{80}$  are a mean for all days of a month and not only for days of clear skies, there is a significant correlation, larger than 0.8, between  $TL_{SRB}$  and  $WV_{160}$  at 160', both over the oceans and the land masses. The relationship between  $TL_{SRB}$  and  $\ln(WV_{160})$  is assessed by the means of statistical regression at the resolution 160'. This relationship is of linear type and is assessed for each month. It appears that a single relation is valid for all months. The correlation between  $TL_{SRB}$  and  $\ln(WV_{160})$  is large (0.85). Only land masses are used for the regression.

Over the oceans, the values  $TL^{TMAP}$  are the best to use a priori. However, we observed some edge effects close to the continents, which lead to very high values of TL. Since the correlation between  $TL_{SRB}$  and  $WV_{160}$  is also large over the oceans, we decided to combine the  $TL^{TMAP}$  and the water vapor in a linear function. The models used are:

for the oceans :

$$TL^*_{80} = 1/2 [ TL^{TMAP}_{80} + (a \ln(WV_{80}) + b)] \quad (22)$$

and for the land masses,  $TL^*_{80} = a \ln(WV_{80}) + b$

where the parameters  $a=1.397$  and  $b=2.486$  are those of the regression between  $TL_{SRB}$  and  $\ln(WV_{160})$ ,

The second iteration deals with orography. To assess the model  $f$ , it is assumed that the relationship between TL and the terrain elevation has the following form:

$$TL(x, y, z) = \exp[\alpha(x, y) - \gamma(x, y) (z/z_H)] \quad (23)$$

where  $\alpha$  and  $\gamma$  are unknowns and  $z_H$  is the scale height for molecules, that is 8435 m. Since TL decreases as the elevation  $z$  increases,  $\gamma$  is positive. At very large elevations, TL tends to 1 since  $\delta$  tends to  $\delta_{Rayleigh}$ . Assuming that at the elevation  $2z_H$ ,  $TL = 1$ , it becomes

$$TL = \exp[\gamma (1 - z/2z_H)] \quad (24)$$

The field of parameter  $\gamma(x, y)$  is assessed at the resolution 80', where both  $TL_{80}$  and  $z_{80}$  are known. Then this field  $\gamma(x, y)$  is resampled at 5' by the means of a bi-cubic spline. Using the same equation as above, an estimate  $TL^*_5$  is computed and provides the high frequencies to be injected in  $TL_{80}$ . A multiresolution synthesis lead to an estimate of  $TL_5$ .

Then,  $TL_5$  is resampled by the means of a multiresolution analysis to obtain the data set  $TL_{20}$ , which will be fused with the sites observations. We found that this procedure provides better results than stopping the synthesis directly at 20', because of the non-orthogonality of the wavelet transform we are using. The analysis is a low-pass filter. The data set  $TL_{20}$  is obtained by re-sampling this analysis by taking one point out of four in each direction.

### 3.3 Interpolation of ground sites and 20' background map

In the second step, it is assumed that the value in a cell of 20' in size should be equal to the mean of those observed for the measuring stations within the cell. The TL of the stations were corrected to the altitude of the cell with equation 7. For all cells containing at least a measuring station, the difference between both data sets is computed ( $d_{TL}$ ). Then, these differences are interpolated by the means of a linear unbiased interpolator. The interpolation method recommended in Lefèvre et al. (2002) is used:

$$\begin{aligned}
 d_{TL}(x) &= \sum w_i d_{TL}(x_i) \\
 w_i &= \left[ (1 - \delta_i) / \delta_i^2 \right] / \sum w_k \text{ with} \\
 \delta_i &= d_i / R \text{ for } d_i < R \\
 w_i &= 0 \text{ otherwise} \\
 \delta_i^2 &= f_{NS}^2 \cdot \left\{ s^2 + [v \cdot (z_2 - z_1)]^2 \right\} \\
 &\text{for } z_2 - z_1 < 1600m \\
 f_{NS} &= 1 + 0.3 \cdot |\Phi_2 - \Phi_1| \cdot [1 + (\sin \Phi_1 + \sin \Phi_2) / 2]
 \end{aligned} \tag{25}$$

$w_i$ : weight  $i$                        $w_k$ : sum of over all weights  
 $R$ : search radius (1600 km)     $v$ : vertical scale factor (500)  
 $s$ : horizontal distance [km]     $h_1, h_2$ : altitudes of the sites [km]  
 $i$ : Number of sites (maximum 6)  
 $\Phi_1, \Phi_2$ : latitudes of the two points

After tests with different ranges, the search radius was set to 1600. The maximum difference added by the second step was limited to 3 TL units.

Additionally the differences  $d_{TL}$  were multiplied with a distance factor in order to avoid jumps at the edges of the interpolation areas:

$$\begin{aligned}
 \text{For } \min(\delta_i) \leq 0.5 \\
 d'_{TL} &= d_{TL} \\
 \text{For } 0.5 < \min(\delta_i) < 1 \\
 d'_{TL} &= d_{TL} \cdot \exp\left\{ - \left[ 4.29 * [\min(\delta_i) - 0.5] \right]^2 \right\}
 \end{aligned} \tag{26}$$

$\min(d_i)$ : distance to the nearest station

Distances up to 800 km are not changed, distances between 800 and 1600 km are decreased smoothly to zero.

Once the field of the residuals is obtained for each cell, this field is added to the gridded data, providing an unbiased gridded map.

## 4. RESULTS

### 4.1 Ground stations

The list of measured and calculated ground stations is given in the Annex Tab. A1. The dataset can be accessed via the prototype of the SoDa project [www.soda-is.org](http://www.soda-is.org).

### 4.2 Maps

The method was applied to the 12 months. Figure 2 shows the original map  $TL_{SRB}$  at resolution 160', while Figure 3 exhibits the synthesized map at resolution 20' for the month of June. TL ranges from 1 (polar regions) to 6 (Amazon basin).

One may note that both maps are similar for large scales. The second one exhibits higher frequencies, which are those found in the external data. A close examination reveals some artifacts that originate from the TMAP or NVAP data.

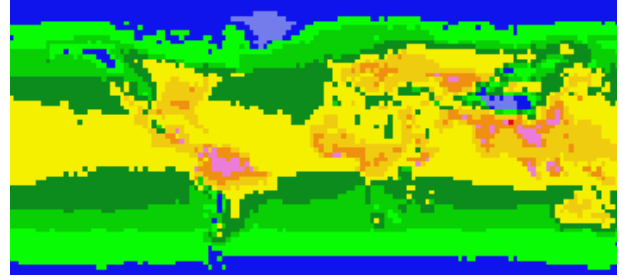


Fig. 2. The original map  $TL_{SRB}$  at resolution 160'. June.

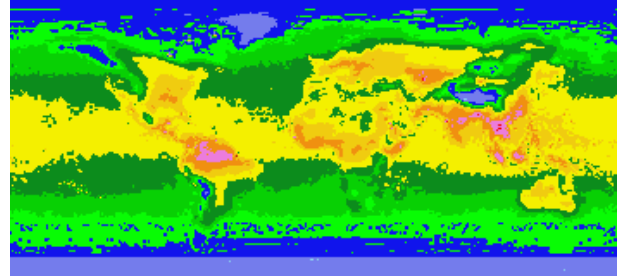


Fig. 3. The synthesized map  $TL_{20}$  at resolution 20'. June.

Interpolated files at 5' and 20' resolution were also calculated: Figure 4 shows the final map at 5' resolution. The maps look spotty, but most of the spots can be explained. Several regional effects like wood burning are not included in the background map but in the ground information. Because of the low density of ground stations (out of Europe and North America) some of the local effects are mapped as spots.

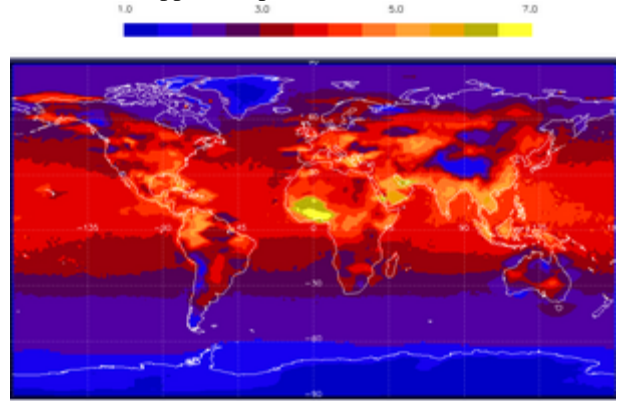


Fig. 4. Corrected TL at surface altitude, resolution 5' for the month of June.

Many tropical stations show high aerosol values just before rainy season, when the wood is burned (e.g. September/October in the Amazonas region). The Sahel zone as well as the region around the Aegaeis Sea shows very high turbidity values during the whole year.

### 4.3 Quality

**4.3.1 Quality of calculation of ground stations.** For several sites results for more than one data source are available. The comparison shows a good agreement between the methods. The standard deviations between the sources and models are about 0.6 TL units (Tab. 3).



Remund J., Wald L., Lefevre M., Ranchin T., Page J., 2003. Worldwide Linke turbidity information. Proceedings of ISES Solar World Congress, 16-19 June, Göteborg, Sweden, CD-ROM published by International Solar Energy Society.

This can also be assumed as the root mean squared error of the ground data. The different sources have not been adapted to one another.

Tab. 3: Differences between different sources. Positive MBEs mean that the second named data is higher.

	N	MBE	RMSE
Hourly beam vs. Daily global radiation	343	0.2	0.6
Hourly beam vs. published measurements	24	0.5	0.7
Daily global radiation vs. published measurements	24	0.3	0.4

4.3.2 *Quality of TL interpolation.* In Tab. 4 the monthly RMSE of the interpolation are listed. Three different RMSE values are listed. The first give the error for the first step of the interpolation. The second gives the error for the interpolation, taking the values of all points into account. The third gives the effective error for the interpolation, not taking the values of the points into account for which the interpolation is made. The RMSE error lies between 0.63 (Dec.) and 0.89 units (March). The second step enhances the quality by about 35%. The RMSE without taking away the measured values is about 0.1–0.3.

The RMSE is influenced a lot by outliers in the tropics - where the distances between sites are very big and the values vary very much in space. About 6 out of 220 grids were eliminated for calculating the effective error.

Tab. 4: Monthly values RMSE of TL at 20' grid.

Month	Sec. Step (all points)		Sec. step (effective error - without outliers)	
	MBE	RMSE	MBE	RMSE
January	-0.03	0.25	0.02	<b>0.67</b>
February	-0.04	0.35	-0.00	<b>0.66</b>
March	-0.04	0.31	-0.06	<b>0.89</b>
April	-0.02	0.19	-0.01	<b>0.73</b>
May	-0.03	0.25	0.01	<b>0.73</b>
June	-0.01	0.15	0.02	<b>0.77</b>
July	-0.01	0.14	0.02	<b>0.77</b>
August	-0.01	0.12	-0.01	<b>0.75</b>
September	-0.03	0.23	-0.02	<b>0.71</b>
October	-0.02	0.20	-0.01	<b>0.73</b>
November	-0.01	0.09	0.04	<b>0.70</b>
December	-0.01	0.15	0.06	<b>0.63</b>
Mean	-0.02	0.20	0.01	<b>0.73</b>

## 5. CONCLUSIONS

The target for accuracy, about 0.6–1 TL value, could be reached. This target may be considered as low. However, it should be stressed that, even in this case, the construction of such maps is a significant step forward the state-of-the-art and that nobody can provide values of the Linke turbidity factor with a much greater accuracy, except at the relatively rare sites where specific observations are made.

**Acknowledgements** - Many thanks goes to H. Gilgen and A. Ohmura of Institute for Atmosphere and Climate ETH (IACETH) for BSRN data and data of Payerne and Reckenholz.

Further we thank the principal investigators Brent Holben and Chuck McClain from GSFC, NASA and Didier Tanre from Univ. Lille for AERONET level 2.0 data.

The Australian Regional Instrument Center, Bureau of Meteorology provided a CD-ROM with global and beam irradiance data of several years. Swiss Meteorological Institute (SMI) provided data of 10 stations and the Swiss Agency for Environment, Forest and Landscape (SAEFL) data of 5 NABEL stations.

This work is supported partly by the programme IST of the European Commission, by the Swiss Federal Office of Energy, Bern (contract No. 79564) and the Swiss Federal Office for Education and Science (contract No. 99.0513).

## REFERENCES

- Beyer H.-G., Czeplak G., Terzenbach U., Wald L., 1997. Assessment of the method used to construct clearness index maps for the new european solar radiation atlas (ESRA). *Solar Energy*, 61, 6, 389-397.
- CNES, 2001 - Centre National d'Etudes Spatiales. POLDER instrument. Web site: <http://www-projet.cst.cnes.fr:8060/POLDER/SCIEPROD/ae9706.htm>, as for August 2001.
- D'Agostino V., A. Zelenka, 1992. Estimating solar global irradiance by integration of satellite and network data: the cokriging approach, *Sci. de la Terre, Sér. Inf.*, **31**, 461-465.
- Daubechies I., 1992. *Ten lectures on wavelets*. CBMS-NSF regional conference series in applied mathematics 61, SIAM, Philadelphia, USA, 357 p.
- DiPasquale, R.C., Whitlock C.H., 1992. Global distribution of shortwave fluxes derived from satellite data for the world climate research programme. *International Journal of Climatology*, **15**, 961-974.
- Dogniaux R. (1974): Representation Analytique des composantes du rayonnement solaire. Institut Royal de Météorologie de Belgique, Serie A No. 83, 1974.
- Dogniaux R. and Lemoine M., 1983. In: W. Palz (Ed.), Solar Energy R&D in the European Community, Series F, Vol. 2, Solar Radiation Data. D. Reidel Publ., Dordrecht, pp. 94-107.

Remund J., Wald L., Lefevre M., Ranchin T., Page J., 2003. Worldwide Linke turbidity information. Proceedings of ISES Solar World Congress, 16-19 June, Göteborg, Sweden, CD-ROM published by International Solar Energy Society.

- ESRA. *European solar radiation atlas*, 2000, includ. CD-ROM. Edited by J. Greif, K. Scharmer. Scientific advisors: R. Dogniaux, J. K. Page. Authors : L. Wald, M. Albuissou, G. Czeplak, B. Bourges, R. Aguiar, H. Lund, A. Joukoff, U. Terzenbach, H. G. Beyer, E. P. Borisenko. Published for the Commission of the European Communities by Presses de l'Ecole, Ecole des Mines de Paris, France.
- Gueymard, C., 1994. Analysis of monthly average atmospheric precipitable water and turbidity in Canada and Northern United States. *Solar Energy*, 53(1), 57-71.
- Gueymard, C.A. and Garrison J.D. (1998): Critical evaluation of precipitable water and atmospheric turbidity in Canada using measured hourly solar irradiance. *Solar Energy Vol 62, No. 4, pp. 291-307, 1998.*
- Holben B.N., D.Tanré, A.Smirnov, T.F.Eck, I.Slutsker, N. Abuhassan, W.W. Newcomb, J.S. Schafer, B Chatenet , F. Lavenu, Y.J.Kaufman, J. Vande Castle, A.Setzer, B.Markham, D. Clark, R. Frouin, R. Halthore, A.Karneli, N. T. O'Neill, C. Pietras, R.T. Pinker, K. Voss, G. Zibordi, 2001. An emerging ground-based aerosol climatology: Aerosol Optical Depth from AERONET, *J. Geophys. Res.*, **106**, 12 067-12 097.
- Kasten F., 1996. The Linke turbidity factor based on improved values of the integral Rayleigh optical thickness. *Solar Energy*, 56 (3), 239-244.
- Jacovides, C.P., 1997. Model comparison for the calculation of Linke's turbidity factor. *International Journal of Climatology*, 17, 551-563.
- King R. and Buckius R.O., 1979: Direct solar transmittance for a clear sky. *Solar Energy* 22, 297-301
- Mallat S. G., 1989. A theory for multiresolution signal decomposition: the wavelet representation. *IEEE Transactions on Pattern Analysis and Machine Intelligence*, 11(7):674-693.
- Meyer Y., 1990. *Ondelettes et opérateurs 1: Ondelettes*. Hermann, Paris, France, 215 p.
- NVAP, 2001 - NASA Water Vapor Project. NASA Langley Research Center Atmospheric Sciences Data Center, Web site: <http://eosweb.larc.nasa.gov>, as of 2001.
- Pedros, R., Utrillas, J.A., Martinez-Lozano, J.A. and Tena, F., 1999. Values of broad band turbidity coefficients in a mediterranean coastal site. *Solar Energy*, 66(1), 11-20.
- Ranchin T. and Wald L., 2000. Fusion of high spatial and spectral resolution images: the ARSIS concept and its implementation. *Photogrammetric Engineering and Remote Sensing*, 66(1), 49-61.
- Remund, J. M. Lefevre, T. Ranchin and L. Wald (2002). Construction maps of the Linke Turbidity factor. SoDa Deliverable D5-2-1. Internal document.
- Randel D. L., Vonder Haar T.H., Ringerud M.A., Stephens G.L., Greenwald T.J., Combs C.L., 1996. A NEW GLOBAL WATER VAPOR DATASET. Bulletin of the AMS (BAMS) - June, 1996 Vol 77, No 6.
- Rapti, A.S. (2000): Atmospheric transparency, atmospheric turbidity and climatic parameters. *Solar Energy Vol. 69, No. 2, pp. 99-111, 2000.*
- Rigollier C., Bauer O., Wald L., 2000. On the clear sky model of the 4<sup>th</sup> European Solar Radiation Atlas with respect to the Heliosat method. *Solar Energy*, 68(1), 33-48.
- TerrainBase, 1995. TerrainBase: Worldwide Digital Terrain Data. Documentation Manual, CD-ROM Release 1.0, April 1995. NOAA, National Geophysical Data Center, Boulder, Colorado, USA.
- TMAP, 2001 - Thermal Modeling and Analysis Project. NOAA Pacific Marine Environmental Laboratory, Web site: [http://las.saa.noaa.gov/las-bin/climate\\_server/dset=AVHRR+PATHFINDER](http://las.saa.noaa.gov/las-bin/climate_server/dset=AVHRR+PATHFINDER), as for August 2001.
- Whitlock C.H., 1995. First global WCRP shortwave surface radiation budget dataset. *Bulletin of the American Meteorological Society*, **76**, 905-922.
- World Meteorological Organization (WMO), 1981. Technical Note No. 172, WMO-No. 557, Geneva, Switzerland, pp. 121-123.
- Zelenka A., Czeplak G., d'Agostino V., Josefson W., Maxwell E., Perez R., 1992. Techniques for supplementing solar radiation network data, Technical Report (3 volumes), International Energy Agency, # IEA-SHCP-9D-1, Swiss Meteorological Institute, Krahbühlstrasse, 58, CH-8044 Zurich, Switzerland.
- Zelenka A., Lazic D., 1987. Supplementing network global irradiance data. In Advances in solar energy technology. In Proceedings of 1986 Biennial Congress ISES Hamburg, Pergamon Press, vol. 4, 3861-3865.







Scr.	Name	Period	Lon	Lat	Alt	Jan	Feb	Mar	Apr	May	Jun	Jul	Aug	Sep	Oct	Nov	Dec
G	Schleswig	1981-90	9.55	54.53	59	2.4	2.1	2.7	2.8	2.9	3.6	3.7	3.4	3.4	-	2.4	2.5
G	Belfast	1981-90	-6.22	54.65	81	2.8	3.0	3.3	3.0	3.7	4.0	4.3	4.4	4.9	-	3.0	2.9
G	Kaunas	1981-90	23.88	54.88	73	2.8	2.1	2.3	1.9	2.0	2.1	2.3	3.0	2.7	2.4	1.9	3.0
G	Annette	1961-90	-131.57	55.03	34	2.6	2.6	3.0	3.0	3.2	3.4	3.4	3.3	3	3.4	2.4	2.1
G	Eskdalemuir	1981-90	-3.2	55.32	242	2.5	2.5	3.1	3.1	3.9	3.6	4.0	4.5	3.9	-	2.6	2.6
G	Taastrup/Kobenhavn	1981-90	12.30	55.67	28	2.0	2.0	2.2	2.8	2.6	3.1	3.6	3.5	3.1	3.0	2.0	2.2
G	Moscwa	1981-90	37.57	55.75	156	2.7	2.5	2.6	2.8	3.3	3.8	3.9	3.6	3.6	3.1	2.4	2.2
P	Thompson	1994-99	97.83	55.78	218	-	-	-	-	3.1	3.7	3.4	3.3	2.7	2.4	-	-
G	Shanwell	1981-90	-2.87	56.43	4	2.4	2.5	3.6	3.5	3.3	3.2	3.8	4.4	3.8	3.6	2.6	2.9
B	Toravere	1999	26.76	58.46	70	-	3.0	3.1	3.3	3.1	3.3	3.0	3.3	3.0	2.6	2.4	-
G	Stockholm	1981-90	18.07	59.35	30	2.5	2.0	2.4	3.0	3.2	3.4	3.5	3.6	3.1	2.7	2.0	-
G	St. Petersburg	1981-90	30.30	59.97	4	1.9	1.9	2.4	2.5	2.6	2.9	2.8	3.1	3.1	2.7	2.0	-
G	Lerwick	1981-90	-1.18	60.13	82	3.3	2.7	3.3	3.2	3.3	3.2	3.9	4.1	4.0	4.1	4.1	-
G	Helsinki	1981-90	24.97	60.37	11	3.0	2.0	2.4	2.7	2.7	2.9	3.0	3.3	3.3	2.9	2.8	-
G	Bergen	1981-90	5.32	60.4	41	-	3.5	3.5	3.3	3.2	3.2	3.5	3.9	3.8	3.6	3.7	-
G	Anchoraga	1961-90	-150.02	61.17	35	2.8	2.5	2.7	2.9	3.7	3.9	3.7	3.9	3.6	3.0	2.8	-
P	Fort Simpson	1971-86	-121.23	61.75	169	2.6	2.6	2.8	3.0	3.0	3.1	3.2	3.2	2.8	2.5	2.3	2.2
G	Valassaaret	1981-90	21.07	63.43	4	-	1.9	2.0	2.3	3.1	3.4	3.6	3.3	3.5	2.5	1.9	-
G	Reykjavik	1981-90	21.9	64.13	52	-	2.0	2.0	2.0	2.1	2.4	2.2	2.3	2.2	2.1	-	-
G	Arkangelsk	1981-90	64.58	64.58	13	-	1.9	2.2	2.0	2.0	2.1	2.2	2.5	2.8	2.2	-	-
A	Bonanza	1995-2000	-148.30	64.73	150	-	-	-	2.5	2.7	2.7	2.7	2.5	2.4	2.3	-	-
G	Fairbanks	1961-90	-147.87	64.82	138	-	2.2	2.1	2.4	3.2	3.7	3.8	3.6	3.3	2.6	2.1	-
G	Lulea	1981-90	22.13	65.55	17	-	1.9	2.0	2.1	2.6	3.0	3.0	3.2	2.7	2.0	-	-
G	Utsjoki Kevo	1981-90	27.03	69.75	107	-	1.9	2.0	2.3	2.5	3.1	3.4	3.9	3.2	2.6	-	-
G	Barrow	1961-90	-156.78	71.3	4	-	2.7	2.2	2.4	2.8	3.6	4.1	-	4.3	3.2	-	-
B	Barrow	1992	-156.61	71.32	8	-	-	-	-	4.7	4.1	3.9	4.0	-	-	-	-
B	Ny Alesund	1993	11.95	78.93	11	-	-	-	2.6	1.8	2.1	-	-	-	-	-	-

\*interpolated because of unreasonably high values